

Effects of the magnetic field penetration into the metal on the Brillouin flow in a crossed-field gap

Cite as: Phys. Plasmas **30**, 012107 (2023); <https://doi.org/10.1063/5.0125449>

Submitted: 12 September 2022 • Accepted: 11 December 2022 • Published Online: 12 January 2023

 Samuel Marini,  Felipe B. Rizzato and  Renato Pakter



View Online



Export Citation



CrossMark

ARTICLES YOU MAY BE INTERESTED IN

[Ion-acoustic feature of collective Thomson scattering in non-equilibrium two-stream plasmas](#)

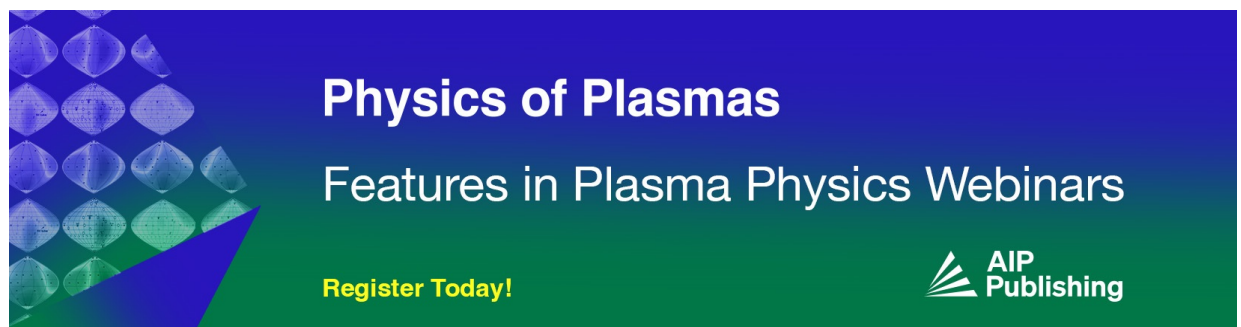
Physics of Plasmas **30**, 012105 (2023); <https://doi.org/10.1063/5.0117812>

[The nonlinear interaction of relativistic laser and hot plasma](#)

Physics of Plasmas **30**, 012106 (2023); <https://doi.org/10.1063/5.0128595>


[Effect of the \$E \times B\$ drift on the redistribution of the divertor particle flux in the HL-2A ECRH plasmas](#)

Physics of Plasmas **30**, 012501 (2023); <https://doi.org/10.1063/5.0126491>



Physics of Plasmas
Features in Plasma Physics Webinars

Register Today!



Effects of the magnetic field penetration into the metal on the Brillouin flow in a crossed-field gap

Cite as: Phys. Plasmas **30**, 012107 (2023); doi: 10.1063/5.0125449

Submitted: 12 September 2022 · Accepted: 11 December 2022 ·

Published Online: 12 January 2023



View Online



Export Citation



CrossMark

Samuel Marini,^{1,2,3,a)} Felipe B. Rizzato,¹ and Renato Pakter¹

AFFILIATIONS

¹Instituto de Física, Universidade Federal do Rio Grande do Sul, Caixa Postal 15051, 91501-970 Porto Alegre, RS, Brazil

²LULI, Sorbonne Université, CNRS, CEA, École Polytechnique, Institut Polytechnique de Paris, F-75252 Paris, France

³CEA, IRFU, DACM, Université Paris-Saclay, 91191 Gif-sur-Yvette, France

^{a)}Author to whom correspondence should be addressed: marini_samuel@yahoo.com.br

ABSTRACT

In this paper, the relativistic Brillouin flow in a crossed-field gap is investigated. For this, the case of a planar magnetron is considered. In contrast to previous studies, it is assumed that the electron discharge occurs in a timescale that is long compared to the magnetic diffusion time in the metal. It is found that the Brillouin flow properties and the overall scenario for the loss of magnetic insulation are different from the short pulse case. In particular, it is shown that two branches of equilibrium Brillouin flow solutions can coexist inside the gap region: one linearly stable and the other linearly unstable. As the parameters are varied, the two branches coalesce and cease to exist in a bifurcation that leads to a complete loss of magnetic insulation. Nevertheless, the mere existence of the unstable solution inside the gap is shown to affect the electron dynamics causing cathode–anode currents. An expression for the onset of the unstable solution is obtained and compared to the relativistic Hull cutoff condition for the short pulse case. It is found that the loss of magnetic insulation occurs for lower accelerating potentials in the present case. This effect is noticeable even for weakly relativistic cases.

Published under an exclusive license by AIP Publishing. <https://doi.org/10.1063/5.0125449>

I. INTRODUCTION

The Brillouin flow is a laminar flow considered as the prevalent steady state in many electron crossed-field devices, such as magnetrons, magnetically insulated line oscillators, and magnetically insulated transmission lines.^{1–6} It is an equilibrium steady state where all the electrons experience no net force.⁷ It can be classified as a single-stream flow because it is a laminar shear flow without orbital crossing. In the Brillouin flow, the electrons in a cross field device are magnetic insulated in the sense that they never reach the anode because the magnetic field force exactly balances the electric forces due to the accelerating potential and the space charge. Therefore, there is no net cathode–anode current, which is a key feature for device operation. Aside from geometry configurations,³ the precise determination of the Brillouin flow depends on the relevant parameters used to describe the specific type of crossed-field device.⁶

In the particular case of magnetrons, the relevant parameters are the accelerating potential V_0 and the magnetic field B_0 because they are both externally applied. The relation between these quantities at which the electrons just graze the anode is called the Hull cutoff condition. In the nonrelativistic regime of interaction, it reads $b_0 = \sqrt{2v_0}$, where $b_0 = eB_0L/mc$ and $v_0 = eV_0/mc^2$ are the normalized magnetic

field and accelerating potential, m and e are the rest mass and charge of the electron, L is the distance between the anode and the cathode (the gap size), and c is the speed of light *in vacuo*.⁸ For magnetic fields that are below this condition, the flow is not magnetic insulated anymore.

Since the 1970s, many studies have been done on the relativistic aspects of the Brillouin flow in a magnetron device.^{2,4,6,9–15} These studies generally assume that the electron discharge occurs in a timescale τ_d shorter than the magnetic field penetration time into the metal $\tau_m = 4d^2\sigma\mu/\pi^2$, where d , σ , and μ are, respectively, the thickness, the conductivity, and the magnetic permeability of the anode.¹⁶ In such a case, the magnetic field becomes trapped inside the gap and its flux is conserved along the discharge.^{17,18} It is shown that in this limit only a single Brillouin flow solution exists inside the gap, and that the Hull cutoff condition at which the electrons graze the anode is given by²

$$b_0 = \sqrt{2v_0 + v_0^2}. \quad (1)$$

As expected, in the low energy limit $v_0 \rightarrow 0$, Eq. (1) leads to the classical Hull cutoff condition. However, as the accelerating potential increases, the relativistic effects demand substantially higher magnetic

fields to guarantee the insulation. In many crossed-field device applications, one needs to operate with magnetic fields that are above but near the Hull cutoff condition. This is, for instance, the case of magnetrons, where to enhance the conversion of beam energy to electromagnetic energy, it is necessary to prevent net cathode–anode current. However, at the same time, the electrons should get close enough to the anode, where their parallel velocity is the largest and might resonate with the slow wave structures.¹²

In this paper, we investigate the electron Brillouin flow in a relativistic magnetron device assuming that the discharge time is long compared to the penetration time of the magnetic field in the metal, i.e., $\tau_d \gg \tau_m$. In this case, the anode becomes transparent to the magnetic field and its magnitude, equal to the externally applied field B_0 . We find that the overall scenario for the loss of magnetic insulation in this case is different from the short pulse case. In particular, we find that two branches of equilibrium Brillouin flow solutions can coexist inside the gap. With the aid of N -particle self-consistent numerical simulations, we are able to determine that one of the branches is linearly stable and, the other, linearly unstable. The two branches coalesce and cease to exist in a bifurcation that occurs inside the gap region. In other words, there is no stable Brillouin flow solution with the electrons grazing the anode. It is also found that the loss of magnetic insulation occurs for higher magnetic fields as compared to the condition given by Eq. (1). This effect is noticeable even for weakly relativistic cases where the pulses are typically longer.

The paper is organized as follows. In Sec. II, we introduce the crossed-field model considered and the equations that describe its dynamics. In Sec. III, we revisit the derivation of the relativistic Brillouin flow and discuss its solutions in the particular case when the magnetic field is assumed to penetrate the electrodes. In Sec. IV, a linear stability analysis of the Brillouin flow solutions is performed. In Sec. V, an N -particle self-consistent code is used to investigate the stationary state achieved by the electrons in the crossed-field device and to determine its magnetic insulation properties. Finally, in Sec. VI, we present our conclusions.

II. MODEL AND BASIC EQUATIONS

The geometry and the electromagnetic field configuration of the relativistic crossed-field gap considered are shown in Fig. 1. It corresponds to a planar magnetron where two long parallel plates oriented in the xz -plane and separated by a distance L along the y -axis are kept at a constant potential difference. The plate at $y=0$ is a grounded cathode and the plate at $y=L$ is an anode kept at an electric potential value V_0 . As a consequence of the electric potential difference, there is a constant external electric field E_0 in the gap region $0 < y < L$. There

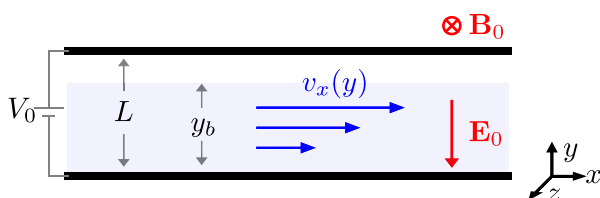


FIG. 1. Schematic diagram of a planar crossed-field gap. The shaded blue region represents the electron flow.

is also a uniform constant externally applied magnetic field B_0 along the z direction.

Given the symmetry of the cathode and the anode plates, we assume that the electron distribution is uniform along that xz -plane, such that all the field quantities only depend on the y coordinate. The electric scalar potential is self-consistently determined from the particle distribution by the Poisson equation

$$\frac{d^2\phi}{dy^2} = \frac{e}{\epsilon_0} n(y), \tag{2}$$

satisfying the boundary conditions $\phi(0) = 0$ and $\phi(L) = V_0$, where $n(y)$ is the electron density. The magnetic field can be derived from a vector potential as $\mathbf{B} = \nabla \times \mathbf{A}$. In the limit when the self-consistent effects of the electron motion on the magnetic field can be neglected, the uniform external magnetic field can be obtained by taking $\mathbf{A} = -B_0 y \hat{x}$. It is clear, however, that as the electrons are accelerated toward the anode, they also gain velocity along the x direction (see Fig. 1). The currents along x create a self-magnetic field that tends to screen B_0 . To properly take into account the self-consistent magnetic effects, the x component of the vector potential has to satisfy

$$\frac{d^2 A_x}{dy^2} = e\mu_0 n(y) v_x(y), \tag{3}$$

with the boundary conditions $A_x(0) = 0$ and $A'_x(L) = B_0$, where $v_x(y)$ is the electron flow velocity along the x direction, and the prime denotes derivative with respect to y . Note that while the boundary condition for A_x at the cathode is arbitrary and was chosen for convenience, the one at $y=L$ guarantees that the magnetic field at the anode is the externally applied B_0 in accordance with the assumption that the electrodes are permeable to the magnetic field.

III. RELATIVISTIC BRILLOUIN FLOW

The relativistic electron dynamics is dictated by the Hamiltonian¹⁹

$$H = c\sqrt{m^2c^2 + [P_x + eA_x(y)]^2 + P_y^2 + P_z^2} - e\phi(y). \tag{4}$$

Since the Hamiltonian does not explicitly depend on x and z , the canonical momentum components P_x and P_z are constants of motion. Their values are determined by the electron velocity when entering the gap region. For a cold injection, $P_x = 0 = P_z$. Note that this condition does not imply that the momentum parallel to the cathode is always zero. In fact, since mechanical and canonical momentum are related by $\mathbf{p} = \mathbf{P} + e\mathbf{A}$, the particles move along the x according to $p_x = eA_x(y)$.

For a stationary state, the electromagnetic fields and the Hamiltonian are time independent. In fact, the Hamiltonian corresponds to the conserved total energy of the particle. For a cold injection and the chosen boundary conditions at the cathode, we find that the constant value of the Hamiltonian is $H = mc^2$ along the electron trajectory. From the constancy of the Hamiltonian, we can readily obtain an expression for the longitudinal momentum as a function of the electromagnetic fields by isolating P_y in Eq. (4),

$$P_y(y) = \pm \frac{\{e^2[\phi^2(y) - c^2 A_x^2(y)] + 2emc^2\phi(y)\}^{1/2}}{c}, \tag{5}$$

where the plus (minus) sign refers to an electron that is moving toward the anode (cathode), and $H = mc^2$ and $P_x = 0 = P_z$ have been used. In the Brillouin equilibrium limit, there is a complete balance of the forces acting on the particles such that they do not move along the y direction. This corresponds to set $P_y(y) = 0$. Using this condition in Eq. (5) and solving for the electric potential, we obtain

$$\phi(y) = \frac{[m^2c^4 + e^2c^2A_x^2(y)]^{1/2} - mc^2}{e}, \tag{6}$$

where we have chosen the physical branch for which $\phi(y) \geq 0$. Substituting this in Eq. (2), we can derive an expression for the electron density as a function of the vector potential and its derivatives that reads

$$n(y) = \frac{c\epsilon_0 [A_x A_x' (m^2c^2 + e^2A_x^2) + m^2c^2 A_x'^2]}{(m^2c^2 + e^2A_x^2)^{3/2}}. \tag{7}$$

From Hamilton's equations, we obtain the transverse velocity as given by $v_x = dx/dt = \partial H/\partial P_x$. Using Eq. (4) and the Brillouin condition $P_y(y) = 0$, this leads to

$$v_x(y) = \frac{e c A_x}{(m^2c^2 + e^2A_x^2)^{1/2}}, \tag{8}$$

where use has been made of $P_x = 0 = P_z$. Substituting Eqs. (7) and (8) in Eq. (3), we finally obtain a closed differential equation for the vector potential for the relativistic Brillouin flow. Isolating the term that depends on second derivative of the vector potential and after some algebra, this equation can be cast in the form

$$\frac{d^2 A_x}{dy^2} = \frac{e^2 A_x}{m^2c^2 + e^2 A_x^2} \left(\frac{dA_x}{dy} \right)^2, \tag{9}$$

where $\epsilon_0 \mu_0 = c^{-2}$ has been used.

Equation (9) can be solved analytically. Dividing the equation by dA_x/dy , we readily notice that both sides can be integrated once. The resulting equation can be cast in the form

$$\frac{dA_x}{dy} = \frac{\kappa}{eL} [m^2c^2 + e^2A_x^2]^{1/2}, \tag{10}$$

where κ is an integration constant to be determined by the boundary conditions. Note that we have conveniently included the eL factor in the denominator such that κ is dimensionless. Equation (10) can be readily integrated once more, leading to

$$A_x(y) = \frac{mc}{e} \sinh\left(\frac{\kappa y}{L}\right), \tag{11}$$

where the boundary condition $A_x(0) = 0$ has already been used to determine the value of a second integration constant. Substituting Eq. (11) in Eq. (6), we obtain a solution for the electric potential

$$\phi(y) = \frac{2mc^2}{e} \sinh^2\left(\frac{\kappa y}{2L}\right). \tag{12}$$

It is clear that the relativistic Brillouin flow electromagnetic field profiles given by Eqs. (11) and (12) are valid inside the electron distribution, i.e., in the region $0 \leq y \leq y_b$. Here, y_b is the so-called hub

height that corresponds to the beam border position, which still has to be determined from the boundary conditions. For any point in the region $y_b \leq y \leq L$, the electron density vanishes. The electromagnetic potentials are then solutions of the one-dimensional Laplace equation obtained by substituting $n(y) = 0$ in Eqs. (2) and (3), subject to the boundary conditions $\phi(L) = V_0$ and $A_x'(L) = B_0$. These solutions are obtained straightforwardly. Since at $y = y_b$ the potentials and their first derivatives have to be continuous, we find that the potentials given by Eqs. (11) and (12) have to satisfy the following conditions at $y = y_b$: $A_x'(y_b) = B_0$, $\phi(y_b) = E_a(L - y_b) + V_0$, and $\phi'(y_b) = -E_a$, where E_a is the electric field at the anode, which is yet unknown. These conditions are used to determine the values of the three unknown variables, namely, y_b , E_a , and κ . In particular, taking the derivatives of Eqs. (11) and (12) with respect to y and imposing the conditions $A_x'(y_b) = B_0$ and $\phi'(y_b) = -E_a$, we can write the first two variables as a function of the third as

$$y_b = \frac{L}{\kappa} \cosh^{-1}\left(\frac{b_0}{\kappa}\right), \tag{13}$$

$$E_a = -\frac{V_0 (b_0^2 - \kappa^2)^{1/2}}{L v_0}, \tag{14}$$

where we have conveniently used the dimensionless parameters $b_0 = eB_0L/mc$ and $v_0 = eV_0/mc^2$. It is worth noting that the equilibrium is completely determined once the parameters b_0 and v_0 are given. Note also that the parameter v_0 measures the relevance of the relativistic effects in the electron flow. Now, evaluating Eq. (12) at $y = y_b$ and using Eqs. (13) and (14) in the condition $\phi(y_b) = E_a(L - y_b) + V_0$, we obtain an equation that determines the values of the variable κ that lead to relativistic equilibrium Brillouin flow conditions. This equation can be cast in the form $f(\kappa) = 0$, where

$$f = \frac{b_0}{\kappa} + \frac{\sqrt{b_0^2 - \kappa^2}}{\kappa} \left[\kappa - \cosh^{-1}\left(\frac{b_0}{\kappa}\right) \right] - 1 - v_0. \tag{15}$$

Once a solution for $f(\kappa) = 0$ is found, we can substitute it in Eqs. (11)–(14) to obtain a detailed description of the relativistic Brillouin flow and its electromagnetic fields.

Since $f(\kappa)$ presents a highly nonlinear dependence on its variable, for a given set of the dimensionless parameters b_0 and v_0 , we need to use numerical methods to determine its roots. In Fig. 2(a), we plot $f(\kappa)$ for the choice of parameters $b_0 = 0.374$ and $v_0 = 0.061$. We

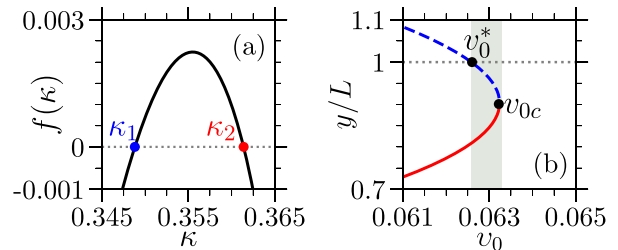


FIG. 2. (a) $f(\kappa)$ given by Eq. (15) presents two real and distinct roots κ_1 and κ_2 when $b_0 = 0.374$ and $v_0 = 0.063$. (b) Maximum y_b/L (hub height) observed at the steady state regime as function of v_0 when $b_0 = 0.374$. The shaded green region corresponds to the values of the parameter where two equilibrium solutions are present inside the gap.

see that the function is non-monotonic and presents two roots located at $\kappa = \kappa_1 \approx 0.349$ and $\kappa = \kappa_2 \approx 0.361$. A quick inspection of Eq. (13) reveals that $y_b(\kappa_1) > y_b(\kappa_2)$. As a matter of fact, for this set of parameters, $y_b(\kappa_1) > L$ such that the only physical solution corresponds to $\kappa = \kappa_2$. Returning to the expression for f in Eq. (15), we notice that the dependence on the parameter v_0 is very simple and only comes in the last additive term $-v_0$. Hence, as v_0 is increased, the curve of $f(\kappa)$ in Fig. 2(a) just moves downward causing its two roots to get closer. At a certain value v_0^* , the root corresponding to κ_1 enters the gap region and the system starts to present two physical equilibrium solutions. Using $y_b = L$ in the expressions for the potentials and their boundary conditions, we can obtain an implicit equation for v_0^* (the critical potential for which the two Brillouin physical solutions emerge) as

$$b_0 = (v_0^* + 1) \cosh^{-1}(v_0^* + 1). \quad (16)$$

Continuing to increase v_0 beyond v_0^* , the two physical solutions get closer and closer until at a certain critical value v_{0c} they coalesce. The critical value can only be computed numerically. For the present case with $b_0 = 0.374$, we find $v_{0c} \approx 0.0635$. For $v_0 > v_{0c}$, the system presents no Brillouin flow solution. In Fig. 2(b), we show the equilibrium hub height y_b as a function of v_0 for $b_0 = 0.374$. In accordance with the discussion above, we see that for $v_0 < v_0^*$, a single solution exists; in the range $v_0^* < v_0 < v_{0c}$, two equilibrium solutions are present; and for $v_0 > v_{0c}$, the systems presents no Brillouin flow equilibrium. For the sake of simplicity, we will denominate the solution corresponding to the lower branch in Fig. 2(b) (solid curve) as y_b , whereas the upper branch solution (dashed curve) will be designated as y_b^* . It is worth noticing that the scenario found here is different from the one found in the case without magnetic field penetration where only a single equilibrium solution exists inside the gap region.²

IV. LINEAR STABILITY

In order to determine the linear stability of the Brillouin equilibrium solutions found in Sec. III, we use an N -particle self-consistent code to describe the electron flow evolution. In the code, the dynamics of each particle is dictated by the Hamiltonian given in Eq. (4), resulting in¹⁹

$$\frac{dy_i}{dt} = \frac{P_y^i}{\sqrt{m^2 c^2 + e^2 (A_x^i)^2 + (P_y^i)^2}}, \quad (17)$$

$$\frac{dP_y^i}{dt} = -\frac{ce^2 A_x^i B_z^i}{\sqrt{m^2 c^2 + e^2 (A_x^i)^2 + (P_y^i)^2}} - eE_y^i(y), \quad (18)$$

where $1 \leq i \leq N$ is the particle label, and N is the total number of particles in the gap region. The electromagnetic fields are computed from Eqs. (2) and (3) using Green's function method.²⁰ Electrons are emitted from the cathode at $y=0$ with a vanishing initial velocity and are removed from the simulation if they return to the cathode or reach the anode.

To test the linear stability, we initialize the electron distribution in the gap according to the prescribed equilibrium density and transverse velocity obtained from Eqs. (7) and (8), where $A_x(y)$ is given by Eq. (11). As a seed for perturbations to grow in the case of an instability, we launch the electrons with a small spread in the longitudinal

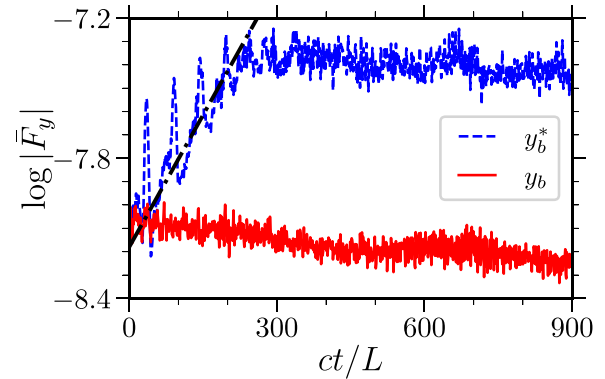


FIG. 3. Time evolution of the mean longitudinal force $|\bar{F}_y|$ measured assuming particles are initially at the hub heights $y_b/L = 0.846$ (solid red line) and $y_b^*/L = 0.961$ (dashed blue line). The results indicate the upper (lower) hub height is linearly unstable (stable). The dotted-dashed line serves as a guide to the eye and indicates an exponential growth of $|\bar{F}_y|$. Here, $b_0 = 0.347$ and $v_0 = 0.063$.

momentum P_y —recalling that in the Brillouin flow all the particles have $P_y = 0$. We initially focus the linear stability analysis on the parameter region where more than one equilibrium solution is present in the gap. In particular, we consider the case with $b_0 = 0.374$ and $v_0 = 0.063$, where equilibrium solutions with hub heights $y_b/L = 0.846$ and $y_b^*/L = 0.961$ exist. To measure if the initial perturbation is increasing, we compute the evolution of the average of the magnitude of the longitudinal force $|\bar{F}_y|$ as the system evolves.²¹ In Fig. 3, we present the results for y_b (solid red line) and y_b^* (dashed blue line) in a linear-log scale. The figure shows that for the equilibrium with the smaller hub height y_b , the net force exponentially decreases with time, indicating a stable solution. On the contrary, for the case with the larger hub height y_b^* , the net force experiences an exponential growth before it saturates at $ct/L \approx 250$, indicating that this solution is linearly unstable.

In Fig. 4, we present snapshots of the normalized $y \times P_y$ phase space obtained from the numerical simulations at the instant of time $ct/L = 0$ (gray dots) and $ct/L = 900$ (red/blue dots). In panel (a), for the case with y_b , we notice that the spread in momentum decreases as the system evolves, tending to the Brillouin flow with all particles

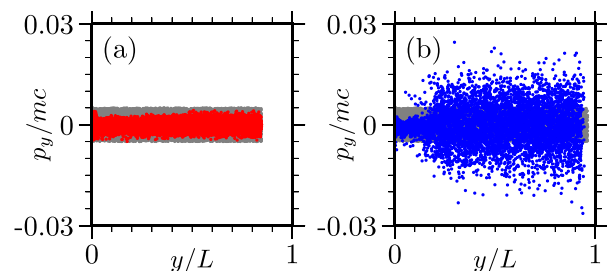


FIG. 4. Snapshots of the electron phase space obtained from the N -particle self-consistent simulations for $b_0 = 0.374$ and $v_0 = 0.063$. The particles are initially launched according to the Brillouin flow equilibrium (gray dots) corresponding to the two existing hub solutions: $y_b/L = 0.846$ in (a) and $y_b^*/L = 0.961$ in (b). The red (blue) dots show the stable (unstable) distribution at the instant of time $ct/L = 900$.

satisfying $P_y = 0$. For the case with y_b^* , panel (b), the scenario is completely different with the instability generating a more complex phase space distribution with an overall larger spread in momentum that has no resemblance with the equilibrium Brillouin flow.

We have also investigated the linear stability for other parameter values, and the general conclusion is that the y_b branch of Fig. 2(b) is always stable, whereas the y_b^* branch is always unstable. Hence, the overall scenario is that the system presents a single stable Brillouin flow solution with a hub height y_b up to $v_0 = v_{0c}$ where a bifurcation occurs as it collides with the unstable y_b^* solution and ceases to exist. This occurs before the stable equilibrium solution reaches the anode. In particular, for $b_0 = 0.374$, we see from Fig. 2(b) that the maximum extent of the equilibrium electron flow corresponds to $y_b/L \approx 0.9$. Again, we note that this is completely different from the case studied in Ref. 2 where the Brillouin flow only ceases to exist when it touches the anode.

V. STATIONARY STATE AND MAGNETIC INSULATION

To investigate the stationary state achieved by a crossed-field device and its magnetic insulation properties, we use the N -particle self-consistent code described in Sec. IV. However, to describe a realistic operation, we now initialize the simulation with an empty gap, $N = 0$, and continuously inject the electrons from the cathode as time evolves. The system eventually reaches a stationary state. This is illustrated in Fig. 5, where snapshots of the normalized $y \times P_y$ phase space at different simulation times for $b_0 = 0.374$ and $v_0 = 0.063$ are presented. These parameters are the same as those used in Figs. 3 and 4, which correspond to a case where the two equilibrium Brillouin flow solutions coexist. For the early times, Fig. 5(a) shows that the electron distribution resembles a ring in phase space. In this stage, as the particles are injected from the cathode they are accelerated by the potential difference, increasing their momentum. Near the middle of the gap, the magnetic force becomes dominant and the electrons start to

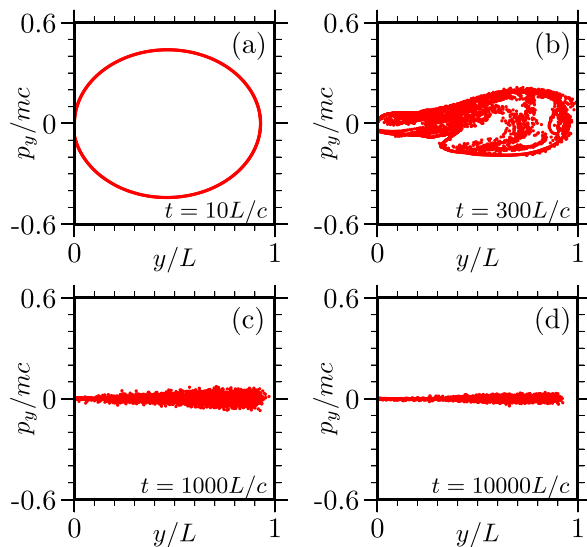


FIG. 5. Electron phase spaces at different instants of time: $t = 10L/c$ (a), $t = 300L/c$ (b), $t = 1000L/c$ (c), and $t = 10000L/c$ (d) assuming $b_0 = 0.374$ and $v_0 = 0.063$. As the electron flow evolves, it approaches the lowest hub height y_b that corresponds to the linearly stable solution.

lose momentum, being reflected before reaching the anode. They eventually return to the cathode with nearly the same momentum as the injection. The ringlike distribution of Fig. 5(a) is nevertheless unstable because small perturbations lead to electron trapping inside the gap.^{22,23} Hence, as the system evolves, particles start to fill the inner region of the ring, distorting it as seen in Fig. 5(b). With further evolution, the electron distribution progressively approaches the stable Brillouin flow predicted by the theory, with a decrease in the momentum spread and the hub height approaching y_b , as seen in Figs. 5(c) and 5(d). We have also compared the electromagnetic field profiles for the stationary state achieved by the simulation with the ones predicted by the theory, and a very good agreement was found. It is worth noting that although the system eventually reaches the stable Brillouin flow solution, the magnetic insulation is not complete. It can be seen in Fig. 5(b) that some particles are reaching the anode and, therefore, leading to a transient net cathode–anode current.

Nevertheless, the normalized magnetic field used in Fig. 5 ($b_0 = 0.374$) is well above the critical one predicted by Eq. (1), namely, $b_0 = 0.360$. This indicates that the penetration of the magnetic field into the metal may lead to a noticeable decrease in the magnetic insulation capability.

To further investigate the issue of magnetic insulation, we have run many numerical simulations for different values of the parameters and computed the normalized integrated cathode–anode current Q_{out}/Q_{in} . All the runs were performed up to the same normalized time $ct/L = 900$. The results are summarized in Fig. 6, where we show Q_{out}/Q_{in} as a function of v_0 for $b_0 = 0.374$. We notice that while Q_{out}/Q_{in} is negligible when only the stable solution is present, it rapidly increases with the presence of the unstable solution in the gap (shaded regions in the figure), becoming nearly the unity once the two solutions bifurcate and cease to exist. Hence, although a stationary cathode–anode current only appears when there are no equilibrium solutions in the gap, we notice that the presence of the unstable solution may be responsible for the onset of transient currents. We therefore can use Eq. (16) as a threshold condition that guarantees a complete magnetic insulation in the case of magnetic field penetration into the metal. We have also performed simulations with other values of b_0 , and the overall scenario is analogous to the one depicted in Fig. 6, such that by increasing (decreasing) the magnetic field, the v_0 value where Q_{out}/Q_{in}

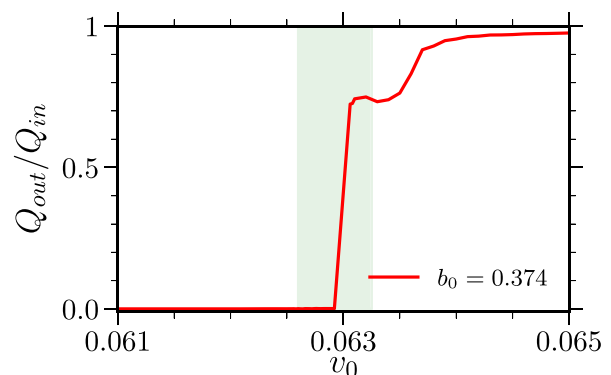


FIG. 6. Q_{out}/Q_{in} as a function of v_0 assuming $b_0 = 0.374$. The shaded green region represents the range $v_0^* < v_0 < v_{0c}$ where two equilibrium solutions are present inside the gap [same as in Fig. 2(b)].

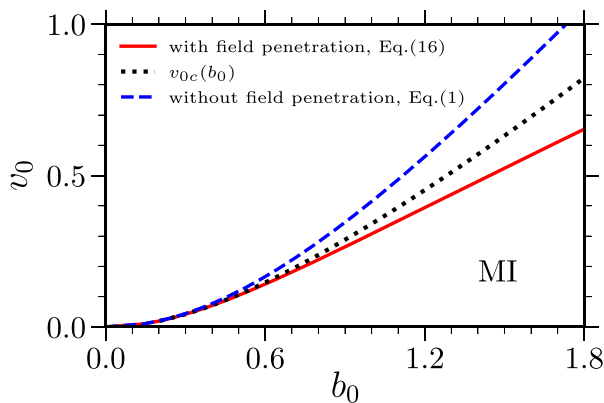


FIG. 7. Critical conditions for the magnetic insulation in the $v_0 \times b_0$ parametric space. The solid red, dotted black, and dashed blue curves correspond, respectively, to $v_0^*(b_0)$ [Eq. (16)], $v_{0c}(b_0)$, and $v_0(b_0)$ [Eq. (1)].

becomes significant is displaced to the right (left). It indicates that a large magnetic field amplitude allows us to further increase the potential difference before the magnetic insulation loss.

In Fig. 7, we compare the different conditions for magnetic field insulation. The solid red curve corresponds to $v_0^*(b_0)$ obtained from Eq. (16), below which a complete magnetic insulation is expected. The dotted black curve shows $v_{0c}(b_0)$, where the two equilibrium solutions collide and cease to exist. Above this curve, there is no insulation with the presence of a stationary cathode–anode current. Finally, the dashed blue curve presents the magnetic insulation condition found in the case of no magnetic field penetration into the metal given by Eq. (1). It is noticeable that the relativistic effects on the magnetic insulation properties are more pronounced in the case of a penetrating magnetic field. This can cause a significant reduction in the region of operation of the crossed-field device.^{10,11} In fact, even for weakly relativistic cases, the penetration of the magnetic field has significant effects. For instance, if we consider an accelerating potential $V_0 = 100$ kV, the increase in the magnetic field to prevent the onset of a stationary cathode–anode current is 10% when compared to the case without penetration into the metal.

VI. CONCLUSIONS

We have investigated the Brillouin flow in a relativistic crossed-field device assuming that the discharge time is long compared to the penetration time of the magnetic field in the metal. We have considered a planar magnetron model and found that the overall scenario for the loss of magnetic insulation is different from the short pulse case where no magnetic penetration into the metal is assumed. In particular, we found that two branches of equilibrium Brillouin flow solutions can coexist inside the gap. Using N -particle self-consistent numerical simulations, we were able to determine that one of the branches is linearly stable and, the other, linearly unstable. The two branches coalesce and cease to exist in a bifurcation that occurs inside the gap region. In other words, there is no stable Brillouin flow solution with the electrons grazing the anode. From the simulations, we observed that the existence of the unstable solution inside the gap may affect the electron dynamics causing cathode–anode currents. Hence, the analytical expression that was obtained for the onset of the

unstable branch, Eq. (16), was used as the critical condition for a complete magnetic insulation and compared to the one obtained in the short pulse case, Eq. (1). It was found that the loss of magnetic insulation occurs for lower accelerating potentials in the case of penetrating magnetic fields. This effect is noticeable even at a weakly relativistic limit. It is anticipated that the penetration of the magnetic field into the metal may play a relevant role in other types of crossed-field devices, such as magnetically insulated transmission lines.^{6,24,25} In that regard, it would be interesting to extend the theory presented here to such different configurations.

ACKNOWLEDGMENTS

This work is supported by CNPq, Brazil. S.M. acknowledges support from Grant No. ANR-11-IDEX-0004-02 Plas@Par, Agence Nationale de la Recherche.

AUTHOR DECLARATIONS

Conflict of Interest

The authors have no conflicts to disclose.

Author Contributions

Samuel Marini: Conceptualization (equal); Investigation (equal); Writing – review & editing (equal). **Felipe Barbedo Rizzato:** Conceptualization (equal); Investigation (equal); Supervision (equal); Writing – review & editing (equal). **Renato Pakter:** Conceptualization (equal); Investigation (equal); Supervision (equal); Writing – original draft (equal); Writing – review & editing (equal).

DATA AVAILABILITY

The data that support the findings of this study are available from the corresponding author upon reasonable request.

REFERENCES

- A. Ron, A. A. Mondelli, and N. Rostoker, “Equilibria for magnetic insulation,” *IEEE Trans. Plasma Sci.* **1**, 85 (1973).
- R. V. Lovelace and E. Ott, “Theory of magnetic insulation,” *Phys. Fluids* **17**, 1263 (1974).
- J. M. Creedon, “Relativistic Brillouin flow in the high v/γ diode,” *J. Appl. Phys.* **46**, 2946 (1975).
- J. Swegle and E. Ott, “Instability of the Brillouin-flow equilibrium in magnetically insulated structures,” *Phys. Rev. Lett.* **46**, 929 (1981).
- C. W. Mendel, Jr., D. B. Seidel, and S. A. Slutz, “A general theory of magnetically insulated electron flow,” *Phys. Fluids* **26**, 3628 (1983).
- Y. Y. Lau, D. A. Packard, C. J. Swenson, J. W. Luginsland, D. Li, A. Jassem, N. M. Jordan, R. D. McBride, and R. M. Gilgenbach, “Explicit Brillouin flow solutions in magnetrons, magnetically insulated line oscillators, and radial magnetically insulated transmission lines,” *IEEE Trans. Plasma Sci.* **49**, 3418 (2021).
- L. Brillouin, “A theorem of Larmor and its importance for electrons in magnetic fields,” *Phys. Rev.* **67**, 260 (1945).
- A. W. Hull, “The effect of a uniform magnetic field on the motion of electrons between coaxial cylinders,” *Phys. Rev.* **18**, 31 (1921).
- E. Ott and R. V. Lovelace, “Magnetic insulation and microwave generation,” *Appl. Phys. Lett.* **27**, 378 (1975).
- A. Palevsky and G. Bekefi, “Microwave emission from pulsed, relativistic e-beam diodes. II. The multiresonator magnetron,” *Phys. Fluids* **22**, 986 (1979).
- A. Palevsky, G. Bekefi, and A. T. Drobot, “Numerical simulation of oscillating magnetrons,” *J. Appl. Phys.* **52**, 4938 (1981).

- ¹²R. C. Davidson, G. L. Johnston, K. T. Tsang, and A. T. Drobot, "Cylindrical Brillouin flow in relativistic smooth-bore magnetrons," *Proc. SPIE* **1061**, 186 (1989).
- ¹³R. C. Davidson, *Physics of Nonneutral Plasmas* (Imperial College Press, London, 2001).
- ¹⁴M. Lopez, Y. Y. Lau, J. W. Luginsland, D. W. Jordan, and R. M. Gilgenbach, "Limiting current in a relativistic diode under the condition of magnetic insulation," *Phys. Plasmas* **10**, 4489 (2003).
- ¹⁵Y. Y. Lau, J. W. Luginsland, K. L. Cartwright, D. H. Simon, W. Tang, B. W. Hoff, and R. M. Gilgenbach, "A re-examination of the Buneman-Hartree condition in a cylindrical smooth-bore relativistic magnetron," *Phys. Plasmas* **17**, 033102 (2010).
- ¹⁶M. Reiser, *Theory and Design of Charged Particle Beams* (Wiley, Weinheim, 2008).
- ¹⁷A. L. Wilmot-Smith, E. R. Priest, and G. Hornig, "Magnetic diffusion and the motion of field lines," *Geophys. Astrophys. Fluid Dyn.* **99**, 177 (2005).
- ¹⁸O. Schnitzer, "Fast penetration of megagauss fields into metallic conductors," *Phys. Plasmas* **21**, 082306 (2014).
- ¹⁹S. Marini, F. B. Rizzato, and R. Pakter, "Space-charge and thermal effects in relativistic crossed-field devices," *Phys. Plasmas* **25**, 063111 (2018).
- ²⁰F. B. Rizzato, R. Pakter, and Y. Levin, "Driven one-component plasmas," *Phys. Rev. E* **80**, 021109 (2009).
- ²¹S. Marini, F. B. Rizzato, and R. Pakter, "Stationary to nonstationary transition in crossed-field devices," *Phys. Plasmas* **23**, 033107 (2016).
- ²²P. J. Christenson and Y. Y. Lau, "Transition to turbulence in a crossed-field gap," *Phys. Plasmas* **1**, 3725 (1994).
- ²³S. Marini, F. B. Rizzato, and R. Pakter, "Thermal effects and space-charge limited transition in crossed-field devices," *Phys. Plasmas* **21**, 083111 (2014).
- ²⁴B. V. Oliver, P. F. Ottinger, T. C. Genoni, J. W. Schumer, S. Strasburg, S. B. Swanekamp, and G. Cooperstein, "Magnetically insulated electron flow with ions with application to the rod-pinch diode," *Phys. Plasmas* **11**, 3976 (2004).
- ²⁵P. F. Ottinger and J. W. Schumer, "Magnetically insulated ion flow theory," *Phys. Plasmas* **13**, 063101 (2006).